



**NIST Special Publication 260**  
**NIST SP 260-245**

# **Certification of Standard Reference Material<sup>®</sup> 640g**

*Line Position and Line Shape Standard for Powder Diffraction  
(Silicon Powder)*

James P. Cline  
Marcus H. Mendenhall  
David Black  
Albert Henins  
Jack B. Prothero

This publication is available free of charge from:  
<https://doi.org/10.6028/NIST.SP.260-245>

**NIST Special Publication 260**  
**NIST SP 260-245**

# **Certification of Standard Reference Material<sup>®</sup> 640g**

*Line Position and Line Shape Standard for Powder Diffraction  
(Silicon Powder)*

James P. Cline  
Marcus H. Mendenhall  
David Black  
*Materials Measurement Science Division (MMSD)*  
*Material Measurement Laboratory (MML)*

Albert Henins  
*Quantum Measurement Division*  
*Physical Measurement Laboratory (PML)*

Jack B. Prothero  
*Statistical Engineering Division*  
*Information Technology Laboratory (ITL)*

This publication is available free of charge from:  
<https://doi.org/10.6028/NIST.SP.260-245>

February 2024



U.S. Department of Commerce  
*Gina M. Raimondo, Secretary*

National Institute of Standards and Technology  
*Laurie E. Locascio, NIST Director and Under Secretary of Commerce for Standards and Technology*

NIST SP 260-245  
February 2024

Certain equipment, instruments, software, or materials, commercial or non-commercial, are identified in this paper in order to specify the experimental procedure adequately. Such identification does not imply recommendation or endorsement of any product or service by NIST, nor does it imply that the materials or equipment identified are necessarily the best available for the purpose.

#### **NIST Technical Series Policies**

[Copyright, Use, and Licensing Statements](#)

[NIST Technical Series Publication Identifier Syntax](#)

#### **Publication History**

Approved by the NIST Editorial Review Board on 2024-02-20

#### **How to Cite this NIST Technical Series Publication**

Cline JP, Mendenhall MH, Black D, Henins A, Prothero JB (2024) Certification of Standard Reference Material® 640g: Line Position and Line Shape Standard for Powder Diffraction (Silicon Powder). (National Institute of Standards and Technology, Gaithersburg, MD), NIST Special Publication 260 (SP) NIST SP 260-245.  
<https://doi.org/10.6028/NIST.SP.260-245>

#### **Author ORCID iDs**

James P. Cline: 0000-0003-0901-2473

Marcus H. Mendenhall: 0000-0001-6236-8212

David Black: 0000-0003-3509-1275

Albert Henins: 0000-0001-6236-8212

Jack B. Prothero: 0000-0002-4766-1741

## Abstract

NIST certifies a suite of Standard Reference Materials (SRMs) to be used to evaluate specific aspects of the instrument performance and measurements via the powder diffraction technique. This includes machines that utilize X-rays, both synchrotron and laboratory-based sources, and neutron powder diffractometers. This report describes the preparation and certification of SRM 640g, the eighth generation of this powder diffraction SRM, which is designed to be used primarily for calibrating powder diffractometers with respect to line position. A unit consists of approximately 7.5 g of silicon powder prepared from intrinsic, float-zone boules. The boules were crushed and ultimately jet milled to a narrow particle size distribution centered on 4 micrometers, and with none smaller than 2.5 micrometers. The powder was then annealed at a temperature and time sufficient to eliminate crystallographic defects. This microstructure engineering allows for the SRM to be used for the determination of the instrument profile function on equipment utilizing laboratory X-ray sources. It can also be used for evaluation of high-resolution equipment; however, advanced data analysis strategies must be employed. The SRM is certified with respect to the lattice parameter, with the SI traceability being through the Cu K $\alpha$  emission spectrum. A NIST-built diffractometer, incorporating many advanced design features, was used to provide data for the certification of the lattice parameter. Both statistical and systematic uncertainties have been assigned to yield a certified value for the lattice parameter at 22.5 °C of  $a = 0.5431109$  nm with an expanded uncertainty ( $k = 2$ ) interval of  $\pm 0.000008$  nm. Prior to comminution, the lattice parameter of single-crystal silicon specimens cut from the boules was measured using the NIST lattice comparator. A value of 0.543102055 nm with an expanded uncertainty ( $k = 2$ ) interval of  $\pm 0.00000027$  nm was obtained.

## Keywords

certification; diffractometer; lattice parameter; powder diffraction; Standard Reference Material (SRM); Système International (SI); silicon.

## Table of Contents

1. Introduction.....	1
2. Material.....	2
3. Experimental.....	5
4. Data Analysis .....	6
5. Statistical Analysis.....	8
6. Conclusions.....	14
7. References .....	15

## List of Tables

Table 1. Certification data for SRM 640g.....	7
Table 2. Peak positions of SRM 640g computed for Cu K $\alpha$ radiation.....	12

## List of Figures

Fig. 1. Data from the left and right beams of delta-d displaying the pendellösung fringes.....	2
Fig. 2. Particle size distribution of SRM 640g. ....	3
Fig. 3. Typical Pawley / FPA fit of SRM 640g. ....	7
Fig. 4. Lattice parameter values vs. sample run order. ....	8
Fig. 5. Autocorrelation plot.....	8
Fig. 6. Autocorrelation permutation test.....	9
Fig. 7. 640g Replicate measurement comparison.....	10
Fig. 8. Sample a vs. b comparison. ....	10
Fig. 9. 640g lattice parameter histogram.....	11
Fig. 10. Normal probability plot of 640g data. ....	11
Fig. 11. Investigation of systematic, type B, error in lattice parameter values. ....	12

## 1. Introduction

The laboratory based divergent-beam X-ray diffractometer can provide a wealth of structural and microstructural information about a wide variety of materials. However, to successfully interpret the data, the operator must have both a properly aligned instrument and take into consideration the aberrations inherent in the para-focusing optics. One method to accomplish this is to use standards to evaluate instrument performance. Non-conventional, synchrotron and neutron-based powder diffractometers also provide data critical to crystallographic and microstructural analyses. While the calibration issues with these machines may be addressed quite differently than those utilizing laboratory X-ray sources, SRMs play a major role in ensuring data integrity from these machines. NIST certifies a suite of SRMs to address specific aspects of powder diffractometer performance. This report describes SRM 640g, the eighth generation of this powder diffraction standard, which is certified with respect to lattice parameter. It consists of approximately 7.5 g of silicon powder specifically prepared to have minimal line broadening and is commonly used for calibrating powder diffractometers for line position and line shape.

## 2. Material

Approximately 103 kg of silicon was purchased from Prex Materials and Sales GmbH, Dorfplatz 7, 84539 Zangberg, Germany. The silicon was supplied in the form of 9 intrinsic, float-zone, boules, 20 cm in diameter and of varying length, with a resistivity of greater than 5000 ohm-cm, that were manufactured by Siltronic AG, Munich, Germany. They ranged in mass from 7 to 16 kg. These silicon boules were analyzed for quality in the as-received state by measuring their lattice spacing on the NIST Silicon Lattice Comparator (delta-d) [1, 2]. The data from this instrument are quite sensitive to the lattice constant (resolution of  $\Delta d/d \approx 6 \times 10^{-9}$ ) and therefore, also to strain and imperfections in the material.

Slices, of approximately 10 mm in thickness, were cut from one end of each boule (9 slices), with both ends being cut from the three largest boules (for a total of 12). From these slices, standard delta-d specimens were prepared, with a thick base and a blade of an initial thickness of  $\approx 500 \mu\text{m}$ . Specimens were cut from the slices on an informal basis to ensure that the entire volume of the boules were represented in the measurements. Using the NIST Center for Nanoscale Science and Technology (CNST) cleanroom facilities, a portion of these pieces were then etched in KOH (80 °C) in an ultrasonic bath for about 30 minutes to remove damage from the cutting operation. The blade thickness was monitored periodically during the etch process using a standard machine-shop micrometer, until the thickness was  $455 \mu\text{m} \pm 5 \mu\text{m}$ . This procedure yielded specimens exhibiting high-quality diffraction patterns on delta-d. Data were collected from a total of 9 specimens. However, owing to the fact that the beams size is much smaller than sample size, if the sample was remounted this constituted a second independent data point. A total of 23 data collection runs were performed on 15 independent regions of the boules.

Delta-d consists of a dual beam, double crystal diffractometer, of Laue geometry that exhibits profiles of nearly non-dispersive breadth. See Figure 1. which shows a typical pair of diffraction peaks from the right-hand and left-hand beams on delta-d. The presence of strong

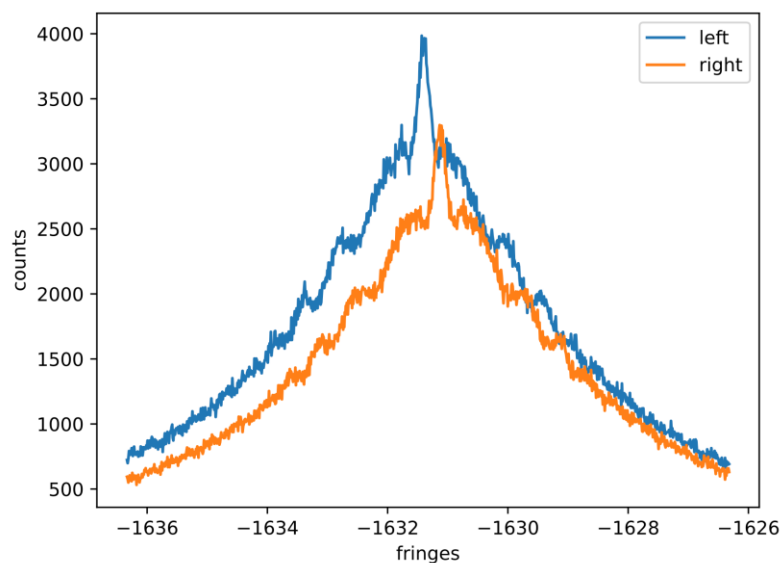


**Fig. 1. Data from the left and right beams of delta-d displaying the pendellösung fringes.**

pendellösung fringes indicates that the material is a nearly perfect crystal, with very low strain and defect density. The dual-beam characteristic of the delta-d instrument allows it to “simultaneously” measure a positive and negative order reflection, which allows the central angle of the crystal to be eliminated. The samples from which data are to be collected using delta-d are mounted on a translation stage such that a specimen and reference crystal can be compared with a single setup. The diffraction patterns were scanned on each crystal, using 0.5 s counting time per step, and an angular step of 10 nrad ( $\approx 1.63 \times 10^{-3}$  seconds of arc). Multiple scans (typically about 10) were carried out on each crystal, and then the translation stage was actuated for analysis of the opposite crystal. This crystal switching procedure was carried out a few times, to allow potential drift of the instrument to be monitored. The apparent d-spacing measurements over time of the specimen were subtracted from a smoothing spline of the apparent d-spacing measurements of the reference crystal, to compute the difference of the lattice spacing of the specimen and the reference. Using the known absolute lattice spacing of the reference crystal, the lattice spacing of the specimen was then computed. The reader is referred to [3] wherein a data-set illustrating this sequence is presented. The outcome was that the material was sufficiently uniform, with a mean lattice parameter of  $0.543102055 \text{ nm} \pm 0.000000027 \text{ nm}$  ( $k=2$  expanded error). The analysis of the samples from the boules of this 103 kg lot of silicon demonstrates that this material is entirely consistent with the data presented in Kessler, *et al.* [2], derived from more than 20 years of analyzing high-resistivity intrinsic float-zone silicon.

Three boules, with a total mass of 40 kg, were then crushed, initially with a large hammer and followed with a jaw crusher, and jet milled to a narrow particle size distribution between 2.5  $\mu\text{m}$  and 6  $\mu\text{m}$ . This comminution was performed on an Alpine 100-AFG jet mill by Hosokawa Micron Powder Systems, Summit, NJ. Typical particle size data from laser scattering measurements (Laser Scattering Particle Size Distribution Analyzer LA-950V2, Horiba, Ltd., Kyoto, Japan) are shown in Figure 2.

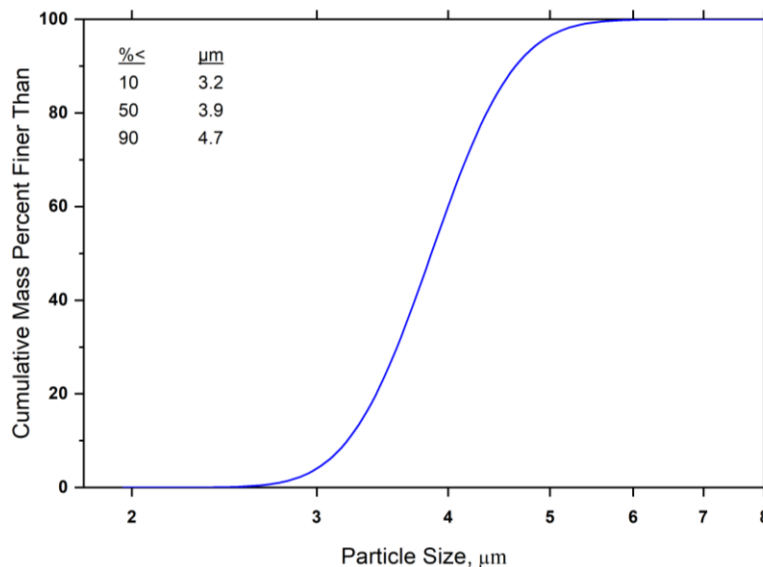


Fig. 2. Particle size distribution of SRM 640g.

The resulting powder was annealed in 51 lots of approximately 575 g each to remove crystallographic defects that would otherwise lead to strain broadening. The annealing was performed in a quartz tube furnace (SH Scientific Co., Ltd, Korea) using quartz boats under flowing, gettered argon (Centorr Associates Model 2B gettering furnace) at a temperature of 1000 °C for one hour [4]. The furnace was evacuated and backfilled with argon three times to minimize oxygen levels before the start of each annealing run. In addition, an oxygen monitor (AEI Technologies, Inc., oxygen sensor S-3A/l) was placed in the outflow from the furnace to monitor oxygen levels within the furnace during annealing. This analyzer has a sensitivity of 0.001 %, and during annealing the oxygen sensor would read zero continuously. Bottling of the silicon powder was performed under argon to protect against humidity.

Given that the starting material was single-crystal, the powder is presumed to consist of single crystal particles. The low end of the size distribution being above 2.5  $\mu\text{m}$  ensured that diffraction data from SRM 640g would display a level of size broadening undetectable with laboratory diffractometers. This combination of controlled particle size and the annealing operation rendered the microstructure of this Si powder appropriate for characterization of the instrument profile function. Procedures associated with this characterization are discussed in [5, 6]; the reader is also referred to Figure 38 therein which compares the full width at half maximum values of various SRMs determined from data collected on a divergent beam instrument.

### 3. Experimental

X-ray powder diffraction data were collected on a NIST-built diffractometer, the divergent beam diffractometer, an instrument that includes several advanced design features. A full discussion of this machine, its alignment and calibration can be found in [5, 6]. The optical layout is that of a conventional divergent-beam Bragg-Brentano diffractometer equipped with a Johansson incident beam monochromator, sample spinner, and a position sensitive detector (PSD). It is also equipped with a 6-axis robot arm configured as an automatic sample changer.

Certification data were collected from 22 samples, 2 samples, denoted as “a” and “b” were prepared using material extracted from each of the 11 randomly selected bottles. The 1.5 kW copper tube of fine focus geometry was operated at a power of 1.2 kW. The variable divergence incident slit was set to a nominal value of  $0.7^\circ$ . A  $1.5^\circ$  Soller slit was located in front of the PSD window to limit axial divergence; no Soller slits were used in the incident beam. The total scan time for each sample was approximately 4.0 hours. The PSD was operated in “picture taking” mode wherein data from the full length of the PSD window were recorded at each position in the scan. The window length was 14.4 mm, which is divided into 192 pixels of  $75\ \mu\text{m}$  each, and with a goniometer radius ( $R$ ) of 217 mm, this corresponds to a  $2\theta$  range of  $3.8^\circ$ , and a  $2\theta$  angular resolution (one pixel) of  $\approx 0.02^\circ$ . The data were recorded using a combination of coarse steps of  $\approx 0.16^\circ\ 2\theta$  and between each coarse step, four fine steps of  $\approx 0.005^\circ\ 2\theta$ , which allowed for both timely data collection and high resolution.

The machine was equipped with an automated anti-scatter slit located directly above the sample center line to prevent air scatter of the incident beam from entering the PSD and contributing to the low angle background. Its height above the specimen was varied as  $\alpha R / (2\cos\theta) + t \tan\theta$  where  $\alpha$  is the full equatorial divergence angle of the incident beam, and  $t$  is a tolerance for longitudinal error in the position of the slit with respect to the center of the beam. The sample was spun at 0.25 Hz during data collection. The diffractometer was located within a temperature-controlled laboratory space where the control of temperature over the time of a run was  $\pm 0.1^\circ\text{C}$ . The temperature was monitored using two 10 k $\Omega$  thermistors with a Hart/Fluke BlackStack system that was calibrated at the NIST temperature calibration facility [7] to  $\pm 0.002^\circ\text{C}$ . The X-ray source was allowed to equilibrate at operating conditions for at least one hour prior to recording any certification data. The performance of the machine was qualified with the use of NIST SRM 660c [8] and SRM 676a [9] using procedures discussed in [5, 6].

#### 4. Data Analysis

Data were analyzed using the Fundamental Parameters Approach (FPA) with Pawley refinements as implemented in TOPAS [10-12]. The FPA method is requisite for analysis of these data as its model accounts for the various optical aberrations of the para-focusing divergent-beam laboratory diffractometer used in this work. While the FPA approach used herein involves several recently developed models, the core of them originated with Wilson [13]. Mendenhall *et al.*, verified that the FPA models as incorporated within TOPAS operated in accordance with published results [14]. The Cu K $\alpha$  emission spectrum for the Cu K $\alpha_1$  source used in this work has been characterized in a manner traceable to the International System of Units (SI) and provides the linkage of the refined lattice parameters to the SI [15, 16]. The optics of the divergent beam diffractometer were modeled as a combination of a Johansson incident beam monochromator and a powder sample using the well-understood behavior of a 2-crystal monochromator, where the sample acts as the second crystal. The resulting “band pass” model provides a “window” function which modifies the intensity of the native copper emission line from the X-ray tube, effectively cutting off the Lorentzian tails, providing good agreement with the shape of the tails of the diffraction peaks. It also adds a dispersion term to the FPA emission model which contributes to the width of the modeled lines, resulting in a better match to the shape of the central part of the diffraction peaks [17].

The parameters associated with the instrument profile function (IPF), the position of the center of the bandpass window, the incident slit angle and the Soller slit angles of the “full” axial divergence model [18, 19], were refined using data from SRM 660c collected at the same time as the certification data. SRM 660c was used to establish these instrument specific parameters since the large attenuation of the LaB<sub>6</sub> minimizes the sample absorption correction providing better characterization of the IPF. These parameters were then fixed at the SRM 660c values for the subsequent analyses of SRM 640g. The sample dependent refined parameters included the scale factors, Chebyshev polynomial terms for the background, the lattice parameters, specimen displacement and attenuation terms, and a term for Lorentzian size broadening. The refined lattice parameter values were adjusted using the coefficient of thermal expansion of silicon [20] to values at 22.5 °C, and are shown in Table 1. A typical plot of the refinement is shown in Figure 3.

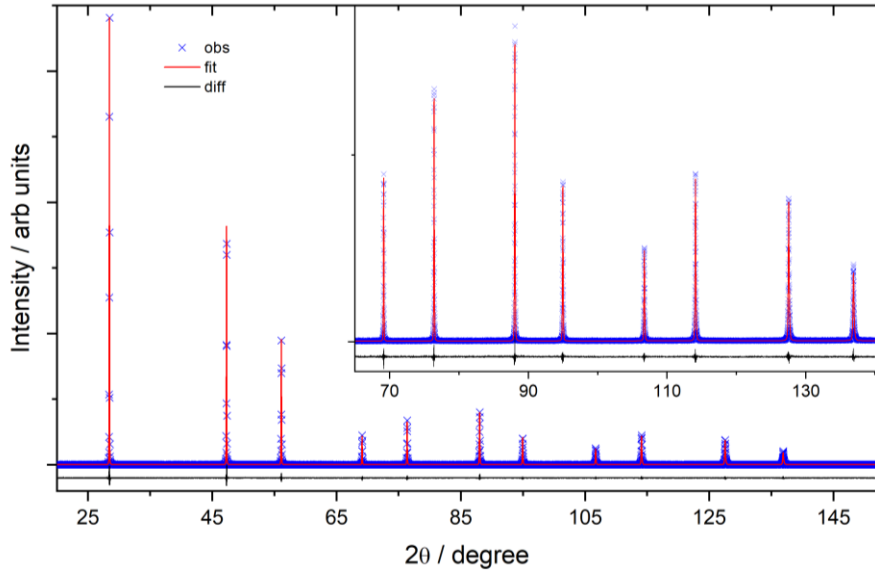


**Fig. 3. Typical Pawley / FPA fit of SRM 640g.**

**Table 1. Certification data for SRM 640g.**

Bottle Number	Lattice Parameter, nm
2765b	0.543 110 86
2309b	0.543 111 86
1478b	0.543 110 87
1123a	0.543 110 63
3460b	0.543 112 62
3154b	0.543 110 68
3460a	0.543 111 13
325a	0.543 111 67
325b	0.543 111 25
1123b	0.543 110 64
3370b	0.543 110 28
688a	0.543 111 14
1890b	0.543 110 26
1a	0.543 109 66
1b	0.543 109 61
2309a	0.543 111 66
688b	0.543 110 97
1478a	0.543 112 29
1890a	0.543 109 29
3154a	0.543 111 05
2765a	0.543 109 95
3370a	0.543 111 83

## 5. Statistical Analysis

Uncertainties in the data were analyzed in the context of both Type A, assigned by statistical analysis, and Type B, based on knowledge of the nature of uncertainties in the measurements, to result in robust uncertainties for the certified values [21-23]. Seven summary plots are generated to examine the potential run order and bottle effects in the observed data for the lattice parameter of SRM 640g.

The first set of three plots evaluates the experimental run order for the potential presence of correlation between measurements that were taken adjacent to one another. Figure 4 displays the measured lattice parameter values in experimental run order as a time series to allow for

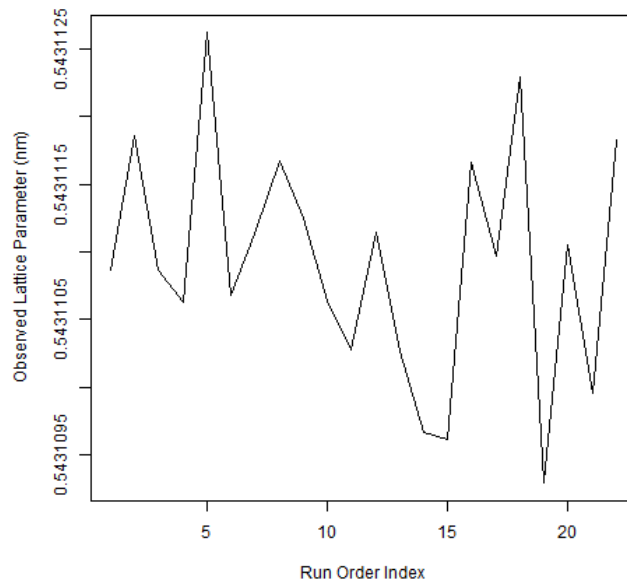


**Fig. 4. Lattice parameter values vs. sample run order.**

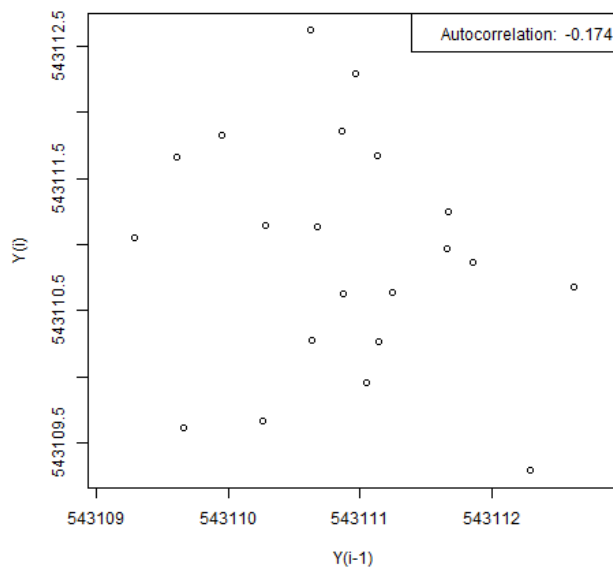


**Fig. 5. Autocorrelation plot.**

a visual inspection for periodic patterns. None are seen. In Figure 5 are the measured lattice parameter values against their immediately preceding values in the run order as a scatter plot. If autocorrelation is not present, we expect the points on this plot to roughly form the shape of a disk, as is observed in Figure 5. The observed autocorrelation between adjacent observations is provided in the legend. Figure 6 displays the results of a permutation test to evaluate the significance of the observed autocorrelation. To conduct this test, we randomly reorder the

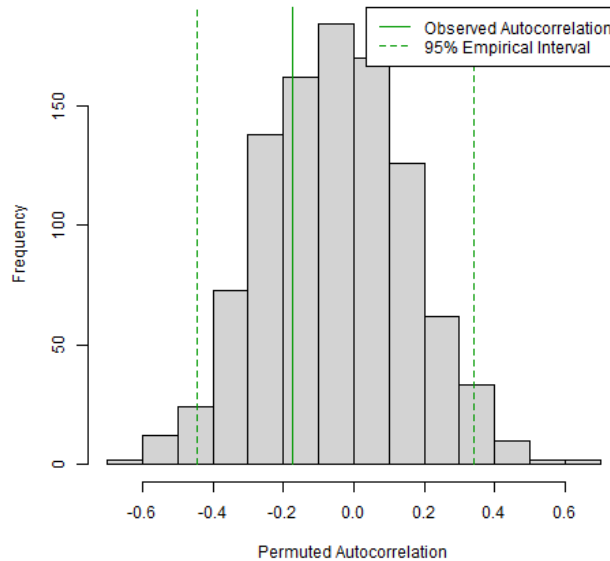


**Fig. 6. Autocorrelation permutation test.**

measurements 1000 times and calculate the resulting autocorrelation between adjacent observations for each random reordering. The histogram in the plot shows the distribution of these 1000 simulated autocorrelations, and the dashed, green vertical lines show the 2.5<sup>th</sup> and 97.5<sup>th</sup> percentiles of the simulated distribution. If the solid, green vertical line representing the original observed autocorrelation falls between the two dashed lines, then the observed autocorrelation is likely not particularly remarkable.

With a second set of plots, the potential bottle number and bottle label effects in the experiments are evaluated. Figure 7 is a plot of the measured parameter values against their bottle numbers, with bottle letter information conveyed via the color & shape of the points. Visually, it is desired to see that “within-bottle” variability and “across-bottle” variability are comparable, as is observed. We can perform an F-test to check if accounting for bottle number explains a significant amount of the total variability seen in the data. The p-value of that F-test appears in the legend of Figure 7, and a value larger than 0.05 can be interpreted as not being able to detect a substantial contribution from bottle number to the overall variability. For this material the p-value is close to 0.05, and we can see visually that some bottles had very low within-bottle variability relative to the overall between-bottle variability. Overall, though, there is not significant statistical evidence that as a whole there are bottle effects to account for in these data.

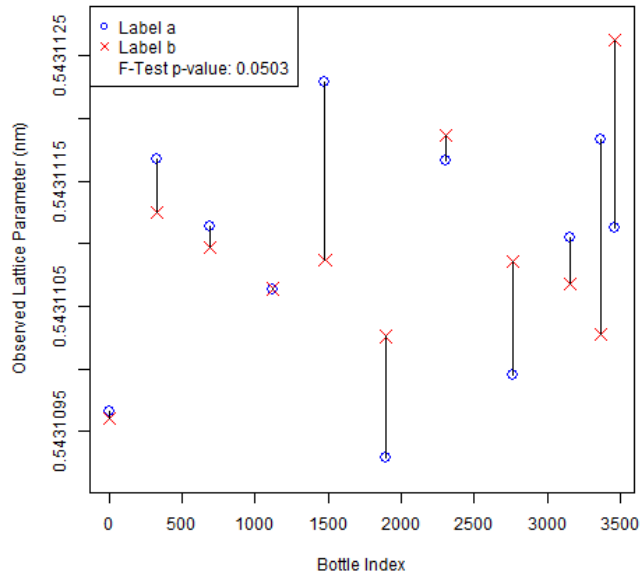


Fig. 7. 640g Replicate measurement comparison.

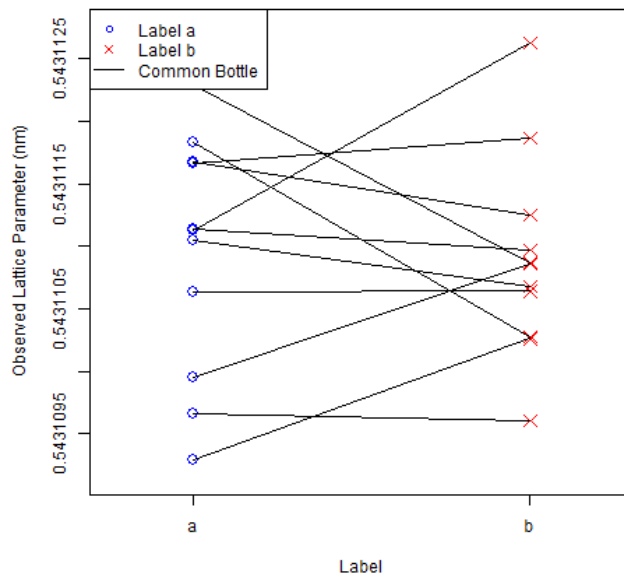
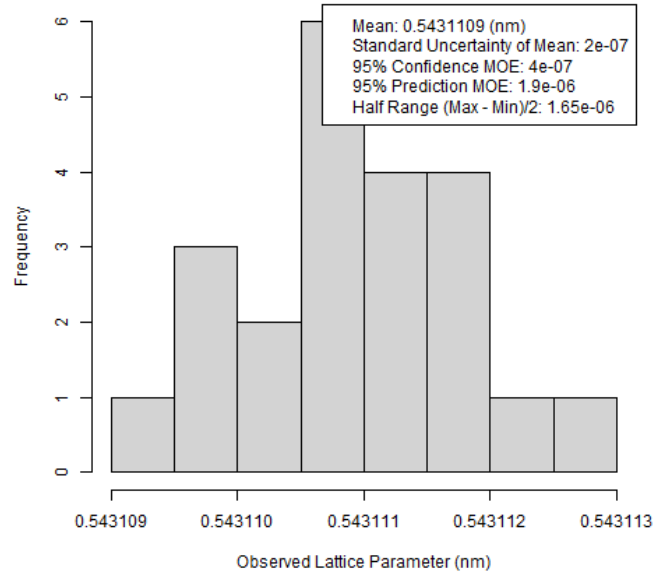


Fig. 8. Sample a vs. b comparison.

In Figure 8 are plotted the measured parameter values against their bottle letters, with observations that share a bottle number connected by a black line. Visually, we're inspecting for substantial differences in center and distribution across the values in each group. For both lattice parameters it appears that bottle number and observation number do not account for substantial amounts of variability in the data. Therefore, we will use a simple average of all the data points to calculate the certified values of the lattice parameters.



**Fig. 9. 640g lattice parameter histogram.**

Figure 9 consists of a histogram of the measured values, and provides the mean, standard uncertainty, and other statistical measures of spread in the legend. A mean lattice parameter value of 0.543 110 92 nm with Type A (K=2) expanded uncertainty of 0.4 fm is realized.

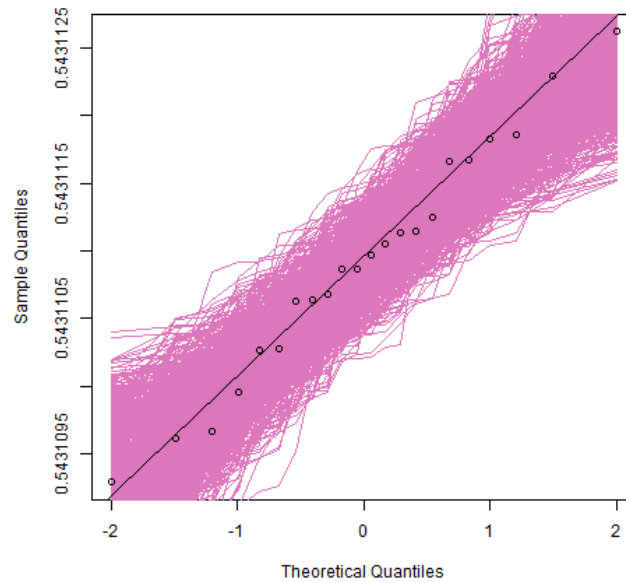


**Fig. 10. Normal probability plot of 640g data.**

As previous tests for autocorrelation and bottle effects all came up negative, we conclude we can use all the measurements directly to compute the certified values. We then plot a Gaussian quantile-quantile plot to check for normality of the distribution of the measured parameter values. The magenta region represents an envelope of typical quantile-quantile plots for Gaussian data. As all the points fall within that envelope and don't demonstrate major

systematic deviation from a linear shape, we don't have evidence to reject Gaussianity for these observations.

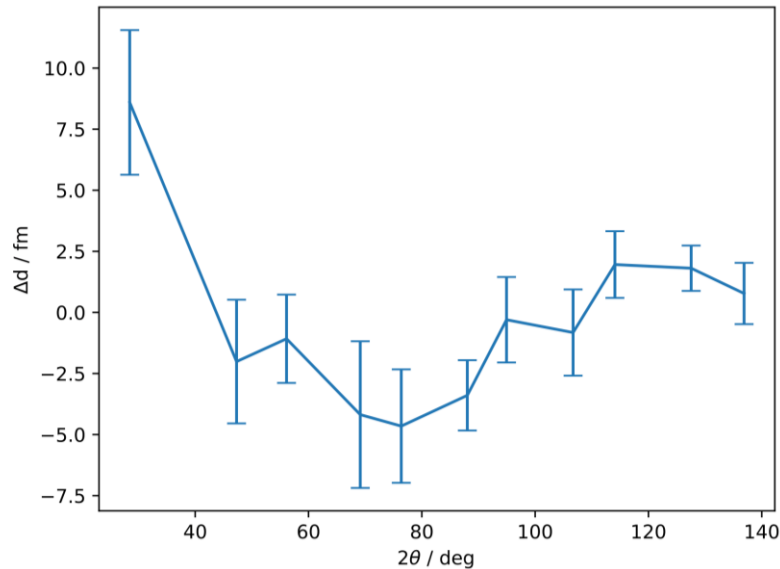


**Fig. 11. Investigation of systematic, type B, error in lattice parameter values.**

Beyond the Type A uncertainty related to the variability of the observations, the measurement process that produced these data also carries with it a Type B uncertainty dependent on the level of systematic error. In the absence of any systematic uncertainty, with the use of the FPA method there would be no variation in the lattice parameters obtained from a whole pattern method, as in Figure 3, and opposed to those obtained from any one of the individual profiles. This would require that the FPA model be operating “perfectly” to correct the reported peak positions for the optical aberrations of the experiment as a function of  $2\theta$ . A more detailed discussion of this issue is given in Black *et al.* [24]. For the analysis presented herein, the certified lattice parameter value is compared with those obtained from the analysis of the individual profiles, with the profile shape terms for each sample frozen at the values obtained from their Pawley refinements. The results from this analysis are shown in Figure 11, with the error bars representing one-sigma. Consideration of these data lead to an assignment of a Type B expanded uncertainty ( $k=2$ ) of  $\pm 0.000\ 008$  nm. Table 2 displays the information values for peak positions computed for SRM 640g using Cu  $K\alpha$  Radiation,  $\lambda = 0.15405929$  nm.

The certified lattice parameter value of 0.543 110 9 nm is significantly larger than the value of 0.543 102 055 nm obtained from the single-crystal boules. This discrepancy is thought to be due to the native oxide layer on the surface of the silicon particles. This surface oxide layer is under compression [25] and therefore produces a hydrostatic tensile stress on the crystallites themselves. This dilates the lattice and leads to the larger measured lattice parameter value for the silicon powder.

**Table 2. Peak positions of SRM 640g computed for Cu K $\alpha$  radiation.**

<i>h</i>	<i>k</i>	<i>l</i>	$2\theta$ (degrees)
1	1	1	28.441
2	2	0	47.301
3	1	1	56.120
4	0	0	69.127
3	3	1	76.373
4	2	2	88.026
5	1	1	94.948
4	4	0	106.703
5	3	1	114.086
6	2	0	127.537
5	3	3	136.883

## 6. Conclusions

The feedstock powder for SRM 640g was prepared from single-crystal boules of intrinsic, float-zone silicon in a manner that ensured high purity and a minimal level of sample induced profile broadening. Prior to comminution, diffraction measurements were performed on the single-crystal material using the “delta-d” diffractometer that verified its suitability for use as an SRM artifact. The SI traceability of the certified lattice parameters was realized through the wavelength of the Cu K $\alpha$  radiation that was used for the powder diffraction experiments. Certification data were collected on a NIST-built laboratory diffractometer equipped with several features that are consistent with its ability to provide metrologically superior data. These data were analyzed in a manner that accounted for the impact of the various optical aberrations of the diffraction geometry used in data collection. Both type A, statistical, and type B, systematic, errors have been assigned to yield a certified value and k+2 expanded uncertainty for the lattice parameter of  $a = 0.357\ 110\ 9\ \text{nm} \pm 0.000\ 008\ 0\ \text{nm}$  at 22.5 °C.

## 7. References

- [1] Kessler EG, Henins A, Deslattes RD, Nielsen L, Arif M (1994) Precision comparison of the lattice parameters of silicon monocrystals. *Journal of Research of the National Institute of Standards and Technology* 99(1):1–18. <https://doi.org/10.6028/jres.099.002>
- [2] Kessler EG, Szabo CI, Cline JP, Henins A, Hudson LT, Mendenhall MH, Vaudin MD (2017) The Lattice Spacing Variability of Intrinsic Float-Zone Silicon. *Journal of Research of the National Institute of Standards and Technology* 122. <https://doi.org/10.6028/jres.122.024>
- [3] Mendenhall MH, Cline JP, Szabo CI, Henins A (2023) The NIST silicon lattice comparator upgrade. *Review of Scientific Instruments* 94(10). <https://doi.org/10.1063/5.0169355>
- [4] van Berkum JGM, Sprong GJM, de Keijser TH, Delhez R, Sonneveld EJ (1995) The optimum standard specimen for X-ray diffraction line-profile analysis. *Powder Diffraction Journal* 10(02):129–139. <https://doi.org/10.1017/S0885715600014512>
- [5] Cline JP, Mendenhall MH, Black D, Windover D, Henins A (2015) The Optics and Alignment of the Divergent Beam Laboratory X-ray Powder Diffractometer and its Calibration Using NIST Standard Reference Materials. *Journal of Research of the National Institute of Standards and Technology* 120:173–222. <https://doi.org/10.6028/jres.120.013>
- [6] Cline JP, Mendenhall MH, Black D, Windover D, Henins A (2019) The optics and alignment of the divergent-beam laboratory X-ray powder diffractometer and its calibration using NIST standard reference materials. in *International Tables for Crystallography*, eds Gilmore CJ, Kaduk JA, & Schenk H (IUCr, Chester, UK), pp 224–251.
- [7] Vaughn CD, Strouse GF (2001) *The NIST Industrial Thermometer Calibration Laboratory. 8th Int'l Symp. Temperature and Thermal Measurements in Industry and Science, Berlin*. Available at [http://ws680.nist.gov/publication/get\\_pdf.cfm?pub\\_id=830734](http://ws680.nist.gov/publication/get_pdf.cfm?pub_id=830734).
- [8] NIST (2015) *Standard Reference Material 660c, Line Position and Line Shape Standard for Powder Diffraction (Lanthanum Hexaboride Powder)*. Available at [https://shop.nist.gov/ccrz\\_ProductDetails?sku=660c&cclcl=en\\_US](https://shop.nist.gov/ccrz_ProductDetails?sku=660c&cclcl=en_US).
- [9] NIST (2015) *Standard Reference Material 676a, Alumina Powder (Quantitative Analysis Powder Diffraction Standard)*. Available at [https://shop.nist.gov/ccrz\\_ProductDetails?sku=676a&cclcl=en\\_US](https://shop.nist.gov/ccrz_ProductDetails?sku=676a&cclcl=en_US).
- [10] Bruker AXS (2017) TOPAS v6, a component of DIFFRAC.SUITE.
- [11] Pawley G (1981) Unit-cell refinement from powder diffraction scans. *Journal of Applied Crystallography* 14(6):357-361. <https://doi.org/10.1107/S0021889881009618>
- [12] Cheary RW, Coelho A (1992) A fundamental parameters approach to X-ray line-profile fitting. *Journal of Applied Crystallography* 25(2):109-121. <https://doi.org/10.1107/S0021889891010804>
- [13] Wilson AJC (1963) *Mathematical Theory of X-ray Powder Diffractometry* (Gordon & Breach).
- [14] Mendenhall MH, Mullen K, Cline JP (2015) An implementation of the Fundamental Parameters Approach for analysis of X-ray powder diffraction line profiles. *Journal of Research of the National Institute of Standards and Technology* 120:223–251. <https://doi.org/10.6028/jres.120.014>

- [15] BIPM (2006) *The International System of Units (SI)* (Bureau International des Poids et Mesures).
- [16] Mendenhall MH, Henins A, Hudson LT, Szabo CI, Windover D, Cline JP (2017) High-precision measurement of the x-ray Cu K $\alpha$  spectrum. *Journal of Physics B: Atomic, Molecular and Optical Physics* 50(11):115004-115004. <https://doi.org/10.1088/1361-6455/aa6c4a>
- [17] Mendenhall MH, Black D, Cline JP (2019) The optics of focusing bent-crystal monochromators on X-ray powder diffractometers with application to lattice parameter determination and microstructure analysis. *Journal of Applied Crystallography* 52(5):1087-1094. <https://doi.org/10.1107/S1600576719010951>
- [18] Cheary RW , Coelho AA (1998) Axial Divergence in a Conventional X-ray Powder Diffractometer. I. Theoretical Foundations. *Journal of Applied Crystallography* 31(6):851-861. <https://doi.org/10.1107/S0021889898006876>
- [19] Cheary RW , Coelho AA (1998) Axial Divergence in a Conventional X-ray Powder Diffractometer. II. Realization and Evaluation in a Fundamental-Parameter Profile Fitting Procedure. *Journal of Applied Crystallography* 31(6):862-868. <https://doi.org/10.1107/S0021889898006888>
- [20] Schoedel R , Boensch G (2001) Precise interferometric measurements at single-crystal silicon yielding thermal expansion coefficients from 12 deg to 28 degC and compressibility. *Lasers in Metrology and Art Conservation*, (SPIE). <https://doi.org/10.1117/12.445624>
- [21] JCGM (2008) *Uncertainty of measurement—Part 3: Guide to the expression of uncertainty in measurement (JCGM 100:2008, GUM:1995)*. Available at <http://www.iso.org/sites/JCGM/GUM-introduction.htm>.
- [22] Taylor BN , Kuyatt CE (1994) *TN1297: Guidelines for Evaluating and Expressing the Uncertainty of NIST Measurement Results*. Available at <https://www.nist.gov/pml/nist-technical-note-1297>.
- [23] Beauchamp C, Camara, J. , Carney, J. , Choquette, S. , Cole, K. , DeRose, P. , Duewer, D. , Epstein, M. , Kline, M. , Lipka, K. , Lucon, E. , Phinney, K. , Polakoski, M. , Possolo, A. , Sharpless, K. , Sieber, J. , Toman, B. , Winchester, M. and Windover, D. (2020) Metrological Tools for the Reference Materials and Reference Instruments of the NIST Material Measurement Laboratory. (Special Publication (NIST SP), National Institute of Standards and Technology, Gaithersburg, MD), 2020-07-15. <https://doi.org/10.6028/NIST.SP.260-136-2020>
- [24] Black DR, Brown CM, Cline JP, Filliben J, Henins A, Mendenhall MH (2020) Certification of Standard Reference Material 660c for powder diffraction. *Powder Diffraction* 35(1):17-22. <https://doi.org/10.1017/S0885715620000068>
- [25] EerNisse EP (2008) Stress in thermal SiO<sub>2</sub> during growth. *Applied Physics Letters* 35(1):8-10. <https://doi.org/10.1063/1.90905>